EFFECT OF WALL PROXIMITY IN FLUID FLOW AND HEAT TRANSFER FROM A SQUARE PRISM PLACED INSIDE A WIND TUNNEL

by

Dipes CHAKRABARTY and Ranajit BRAHMA

Original scientific paper
UDC: 532.54:536.24
BIBLID: 0354-9836, *11* (2007), 4, 65-78

Experimental investigations in fluid flow and heat transfer have been carried out to study the effect of wall proximity due to flow separation around square prisms. Experiments have been carried out for the Reynolds number $4.9 \cdot 10^4$, blockage ratios are 0.1, 0.2, 0.3 and 0.4, different height-ratios, and various angles of attack. The static pressure distribution has been measured on all faces of the square prisms. The results have been presented in the form of pressure coefficient, drag coefficient for various height-ratios and blockage ratios. The pressure distribution shows positive values on the front face whereas on the rear face negative values of the pressure coefficient have been observed. The positive pressure coefficient for different height-ratios does not vary too much but the negative values of pressure coefficient are higher for all points on the surface as the bluff body approaches towards the upper wall of the wind tunnel. The drag coefficient decreases with the increase in angle of attack as the height-ratio decreases. The maximum value of drag coefficient has been observed at an angle of attack nearly 50° for square prism at all height-ratios. The heat transfer experiments have been carried out under constant heat flux condition. Heat transfer coefficients are determined from the measured wall temperature and ambient temperature, and presented in the form of Nusselt number. Both local and average Nusselt numbers have been presented for various height-ratios. The variation of local Nusselt number has been shown with non-dimensional distance for different angles of attack and blockage ratios. The variation of average Nusselt number has also been shown with different angles of attack for blockage ratios. The local as well as average Nusselt number decreases as the height-ratio decreases for all non-dimensional distance and angle of attack for square prisms. The average Nusselt number for square prisms of different blockage ratio varies with the angle of attack. But there is no definite angle of attack at different blockage ratio at which the value of average Nusselt number is either maximum or minimum.

Key words: *flow separation, square prism, blockage ratio, height-ratio, angle of attack, pressure coefficient, drag coefficient, nusselt number*

Introduction

Many investigations have been carried out for heat transfer by forced convection between the exterior surface of bluff bodies such as spheres, cylinder, and square, trian-

gular and rectangular prisms. The important characteristics of flow over a bluff body lie in the nature of the boundary layer. As the streamlines pass over a bluff body, separation takes place due to excessive loss of momentum at adverse pressure gradient from a point, which is not far from the leading edge of the bluff body. The study of fluid flow and heat transfer from a bluff body is important in number of fields such as heat exchanger, gas turbine blades, hot wire anemometry and cooling of electronic equipments, vehicle aerodynamics, and building aerodynamics. This research is also useful for validation of numerical codes for calculation complex flows with huge experimental database on drag force and heat transfer.

By extensive search of literature it is revealed that fluid flow over different shaped bluff bodies like square, triangular, circular, rectangular, and toroids has been investigated thoroughly [1-8]. Igarashi [5] has investigated the flow characteristics around a square prism at an angle of attack (0° α 45°) in the range of subcritical Reynolds numbers. The flow characteristics can be subdivided according to the magnitude of angle of attack (1) 0° α 5°: perfect separation type symmetric flow, (2) 5° α 13°: perfect separation type, unsymmetric flow, (3) 14° ~ 15° α 35°: reattachment flow type, and (4) 35° < α 45°: wedge flow. The flow pattern is closely related to the r.m.s. value of fluctuating pressure. Literatures are also available for heat transfer from different geometric shaped bluff bodies at various conditions like various angles of attack and Reynolds numbers [9-19]. Igarashi [15] have studied the local as well as average heat transfer from a square prism to an air stream in the range of subcritical Reynolds number. He has observed that the average heat transfer has a minimum value at an angle of attack (α) equal to 12-13° and a maximum value at α = 20-25°. From the various literatures it appears that the experimental investigations on fluid flow and heat transfer studies considering the wall effect (*i. e*. by varying the distance from the wall) with different angles of attack as well as different locations on square prisms have not been adequately covered. In the present work experimental investigations are carried out to determine the pressure and drag coefficients from the measurement of the pressure distributions around the square prisms and the average heat transfer rates from the prism as influenced by (1) Reynolds number, (2) angle of attack, (3) blockage ratio, and (4) ratio of the distance of the centroid of the bluff body from the upper wall to the height of the test section in the wind tunnel.

Experimental technique

The schematic diagram and the photographic view of the experimental set-up are shown in figs. 1 and 2, respectively. The experimental set-up consists of wind tunnel driven by an axial flow fan; the wind tunnel is on the pressure side of the fan and the model within the test section of the wind tunnel. The experiment has been carried out in a low speed wind tunnel with a working section 300 mm high, 150 mm wide, and 800 mm long. The test model has been fitted along the width of the test section. There is a slotting arrangement along the sidewall of test section of the wind tunnel for lifting the bluff body from the center towards the upper wall of the wind tunnel to investigate the wall effect on

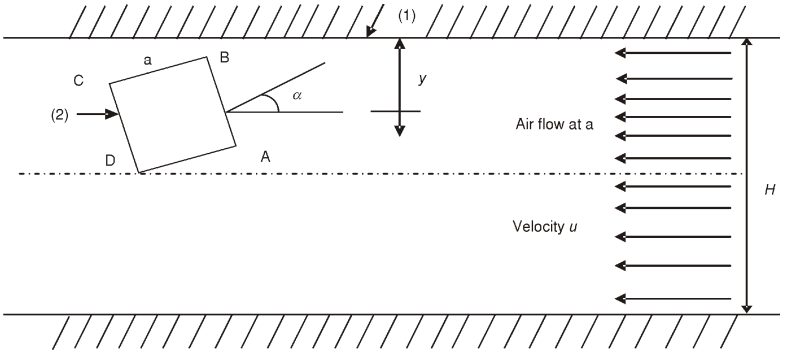

Figure 1. Schematic diagram of the experimental set up
(1) upper wall of the wind tunnel; (2) square prism (BC = a)

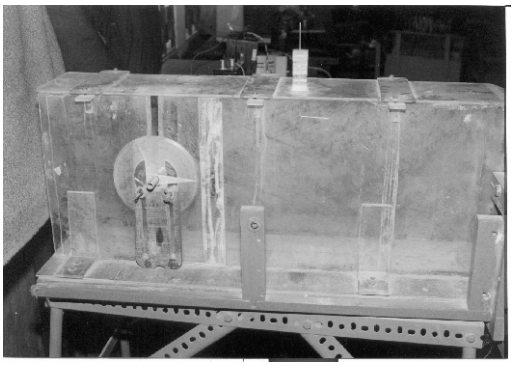

Figure 2. Photographic view of the experimental set up

fluid flow and heat transfer characteristics. The approach velocity of the undistributed flow has been measured by a Pitot tube. The Pitot tube has been placed inside the wind tunnel facing the direction of airflow. A protractor is attached with the bluff body and is fitted at the sidewall of the wind tunnel to measure the angle of rotation of the bluff body. The bluff body rests on the both sides of the sidewall of the wind tunnel by a hollow mild steel pipe from the extension of the inside of the bluff body. The square prisms for the fluid flow experiment are made of perspex sheet of 2.5 mm thickness. The side of the four prisms are of 30, 60, 90, and 120 mm and the length of the prisms are 140 mm. On each face of the 30, 60, 90, and 120 mm side prism, in the mid-span of the prism are drilled 5, 6, and 4 holes each of 1 mm diameter, respectively. The position of the holes on each face of the prisms are for 30 mm side prism: 5, 10, 15, 20, and 25 mm (x/a = 0.167, 0.333, 0.5, 0.667, and 0.833); for 60 mm side prism: 5, 15, 25, 35, 45, and 55 mm (x/a = = 0.083, 0.25, 0.417, 0.583, 0.75, and 0.917); for 90 mm side prism: 5, 20, 35, 50, 65, and 80 mm (x/a = 0.056, 0.222, 0.389, 0.556, 0.722, and 0.889), and for 120 mm side prism: 5, 35, 80, and 110 mm (x/a = 0.042, 0.292, 0.667, and 0.917) from the edge of each face. Stainless steel tubes of 1 mm outside diameters are fitted in these tapping and they are connected to a multitube manometer by flexible tubes for measurement of static pressure distribution. The measurements are taken for the following parameters: (a) angle of attack α = 0-85°, (b) blockage ratio a/H = 0.1, 0.2, 0.3, and 0.4, (c) height ratio y/H = 0.5, 0.350, 0.217, 0.167, and 0.083, and (d) Reynolds number = $4.9 \cdot 10^4$.

The heat transfer experiment has been done under constant heat flux condition. Constant heat flux condition has been maintained by supplying electrical power to the heating foils. The square prisms of heat transfer experiment are made of bakelite. Sufficient insulation has been provided to minimize the heat loss. Stainless steel foils of 0.03 mm thickness have been used for the purpose of producing constant heat flux. The foils are polished to minimize the heat loss due to radiation. The foils are connected with copper strip on both sides through which the power is supplied. The purpose of the present investigation is to measure the local wall temperature distribution at steady state condition at different points for calculation of local as well as average heat transfer coefficient and Nusselt number. Calibrated copper-constantan thermocouples on 30, 60, 90, and 120 mm side prism are embedded on each face in 2, 3, 4, and 4, respectively. The positions of the thermocouples on each face of the prisms are for 30 mm side prism: 10 and 20 mm (x/a = 0.333, 0.667); for 60 mm side prism: 20, 30, and 40 mm (x/a = 0.333, 0.5, and 0.667); for 90 mm side prism: 15, 35, 55, and 75 mm (x/a = 0.167, 0.389, 0.611, and 0.833); and for 120 mm side prism: 15, 45, 75, and 105 mm (x/a = 0.125, 0.375, 0.625, and 0.875) from the edge of each face. The copper-constantan thermocouple beads are soldered at the relevant points on the stainless steel foils. Since the size of the thermocouple beads (d = 0.5 mm) are very small, so the temperature difference between the plate and surrounding air is also very small (in the order of 22-30 °C). So, the error in the temperature measurement is also likely to be very small. This is a widely used technique for temperature measurement for constant heat flux condition. The thermocouple wires are brought out through one end-side of the prism and connected to a digital micro-voltmeters via a selector switch. There is an arrangement for giving power supply to different faces of the prism through a variable transformer so that the experiment can be conducted for different heat inputs. Voltmeters and ampermeters have measured the voltage drop and current across the stainless steel foils, respectively.

Results and discussions

Fluid flow characteristics

The flow characteristics around a square prism have been studied by measuring the pressure distribution on different faces of the prism. From the results it is observed that the pressure distribution varies with the size of the prism as well as with the position of the bluff body with respect to the upper wall. It has been found that the pressure distribution varies considerably with the angle of attack. As the air flows over the prism, the front faces show positive pressure coefficient and the flow separation occurs at the rear face causing negative pressure coefficient. For determination of pressure coefficient C_p, the pressure difference $p - p_a$ has been non-dimensionalised by dividing with $0.5\,\rho_a u^2$ of the air. Figures 3 to 10 shows the variation of pressure coefficient with non-dimensional distance at different height-ratio (*i. e.* y/H = 0.5, 0.350, 0.217, 0.167, and 0.083). The value of the Reynolds number is taken as $4.9 \cdot 10^4$ in all plots. For, fig. 3 ($\alpha = 0°$, a/H = = 0.1) the value of positive pressure coefficient is almost same for all points of the surface

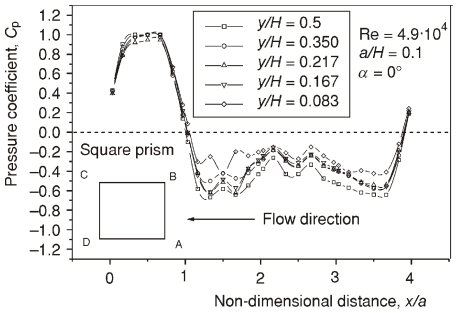

Figure 3. Variation of pressure coefficient with non-dimensional distance at different height-ratios of a square prism (a/H = 0.1, α = 0°)

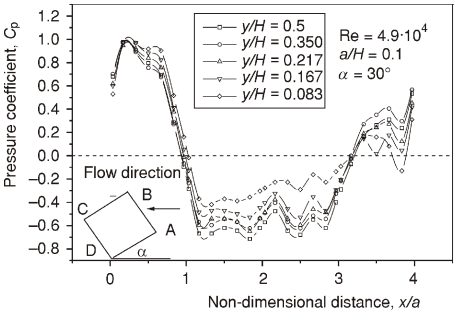

Figure 4. Variation of pressure coefficient with non-dimensional distance at different height-ratios of a square prism (a/H = 0.2, α = 30°)

for different *y/H*. The maximum value of positive C_p is found more or less at the middle point of the front face of the prism (*i. e.* the face in front of the direction of the flow at α = 0°). The negative pressure coefficients are less for *y/H* = 0.5 than *y/H* = 0.083. The values of (–ve) C_p for *y/H* = 0.350, 0.217, and 0.167 are more or less same for almost all points on the surface. For, fig. 4 (α = 30°, *a/H* = 0.1) the positive C_p is very slightly higher or almost same for lesser value of *y/H* at different points. The negative C_p is higher for decreasing value of *y/H*. The flow reattaches at the lower side face for α = 30°, gives positive value of C_p. Figure 5 shows the variation of pressure coefficient in different faces of square prism at various height-ratios (y/H = 0.5, 0.350, 0.217, and 0.167) for blockage ratio *a/H* = 0.2, at Re = 4.9·10^4, the values of (+ve) C_p are almost same for all *y/H* and negative values of C_p are greater at lesser value of height-ratio. For α = 30° (fig. 6) the negative value of pressure coefficient has a markedly difference for all points of pressure tapping with the decreasing value of height-ratio. Figures 7 and 8 shows the plot of C_p *vs*.

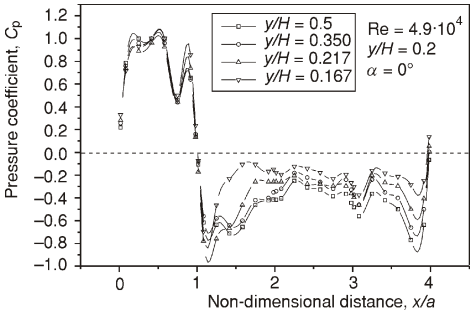

Figure 5. Variation of pressure coefficient with non-dimensional distance at different height-ratios of a square prism (a/H = 0.2, α = 0°)

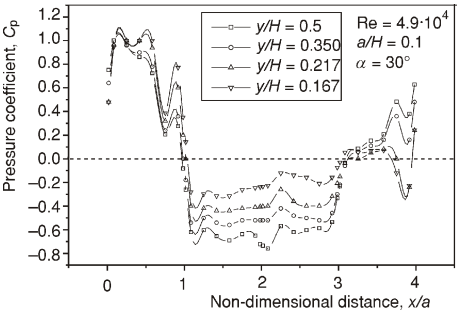

Figure 6. Variation of pressure coefficient with non-dimensional distance at different height-ratios of a square prism (a/H = 0.2, α = 30°)

x/a for $a/H = 0.3$, Re = $4.9 \cdot 10^4$ where $\alpha = 0°$ and 30°, respectively, at different height-ratios. For, fig. 7 ($\alpha = 0°$) and fig. 8 ($\alpha = 30°$) the positive values of C_p are almost same for different values of y/H but the negative value of that are higher for $y/H = 0.350$ than $y/H = 0.5$. At $\alpha = 0°$ and 30° the pressure distribution for different height-ratio on different

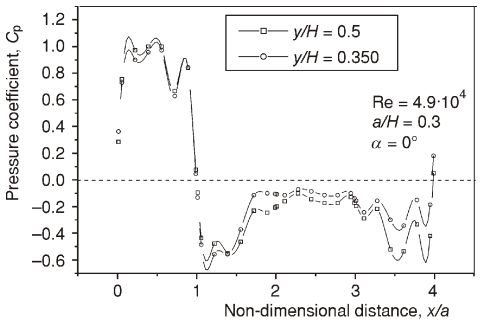

Figure 7. Variation of pressure coefficient with non-dimensional distance at different height-ratios of a square prism ($a/H = 0.3$, $\alpha = 0°$)

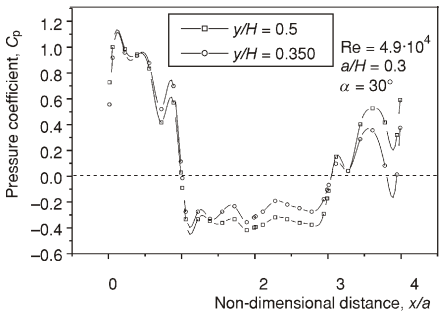

Figure 8. Variation of pressure coefficient with non-dimensional distance at different height-ratios of a square prism ($a/H = 0.3$, $\alpha = 30°$)

faces of the prism are shown in figs. 9 and 10 for $a/H = 0.4$ and Re = $4.9 \cdot 10^4$. For $\alpha = 0°$ and 30° the positive and negative values of C_p are slightly higher at almost all points of the surface for $y/H = 0.350$ than $y/H = 0.5$ but at some points the values of C_p are greater for $y/H = 0.5$ than $y/H = 0.350$.

Drag force (F_D) has been calculated by integrating the pressure distribution in the direction of airflow on the four faces of the square prism. For calculation of drag coefficient C_D, the drag force F_D has been divided by $0.5\rho_a u^2 A$, where A is the surface area

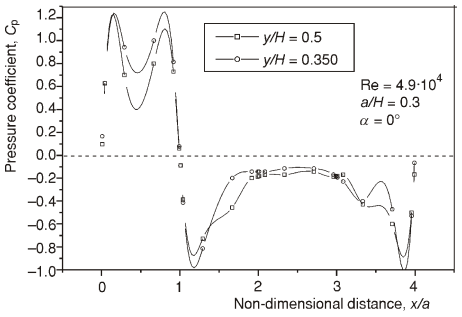

Figure 9. Variation of pressure coefficient with non-dimensional distance at different height-ratios of a square prism ($a/H = 0.4$, $\alpha = 0°$)

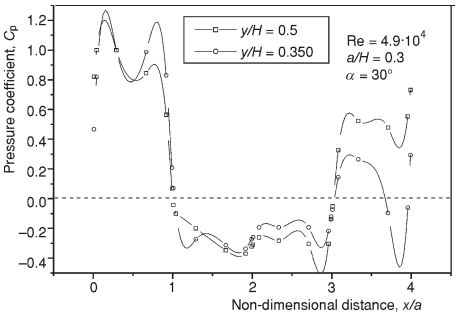

Figure 10. Variation of pressure coefficient with non-dimensional distance at different height-ratios of a square prism ($a/H = 0.3$, $\alpha = 30°$)

of the bluff body. Figures 11-14 shows the variation of drag coefficient (C_D) with the angle at attack α for different height-ratio y/H at Re = $4.9 \cdot 10^4$ where $a/H = 0.1$, 0.2, 0.3, and 0.4, respectively. From fig. 11 it is seen that for all y/H, C_D is maximum at an angle of attack of 50°, it increases from 0-50° and then decreases from 50-85°. It is also observed that as the value of y/H decreases, the value of C_D also decreases for all angles of attack, *i. e.* when the body has been approaching towards the upper wall the value of drag coefficient decreases. In fig. 12, the value of C_D is maximum at $\alpha = 40°$ for $y/H =$ = 0.5 and 0.350 and at $y/H = 0.217$ and 0.167, C_D is maximum at $\alpha = 50°$ and the value

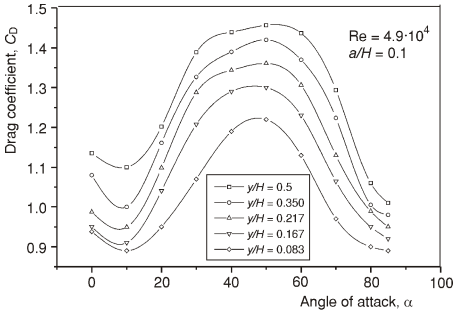

Figure 11. Variation of pressure coefficient with non-dimensional distance at different height-ratios of a square prism (a/H = 0.1)

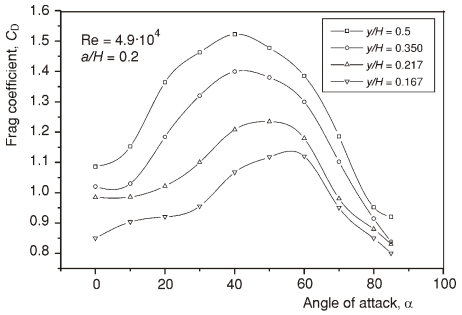

Figure 12. Variation of drag coefficient with angle of attack at different height-ratios of a square prism (a/H = 0.2)

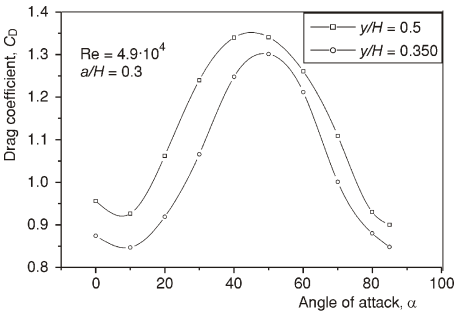

Figure 13. Variation of drag coefficient with angle of attack at different height-ratios of a square prism (a/H = 0.3)

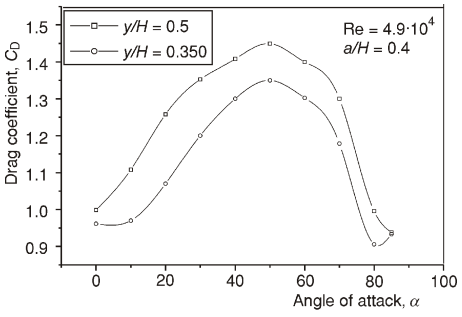

Figure 14. Variation of drag coefficient with angle of attack at different height-ratios of a square prism (a/H = 0.4)

of C_D decreases as y/H decreases. Figure 13 shows C_D *vs.* α graph at $a/H = 0.3$ and Re = $4.9 \cdot 10^4$. Comparison for two height-ratios (*i. e.* y/H = 0.5 and 0.350) is shown here. The maximum value of C_D have been observed at $\alpha = 50°$ and the graph increase from 0 to 50° and then decreases from 50 to 85°. Figure 14 shows the variation of C_D

with α for different *y/H* at Re = $4.9 \cdot 10^4$ at a blockage ratio = 0.4. Here also maximum value of C_D have been observed at $\alpha = 50°$.

From the plot between pressure coefficients *vs.* non-dimensional distance, it is observed that as the body approaches towards the upper wall, the negative pressure coefficient as well as the plot from drag coefficient *vs.* angle of attack, the drag coefficient decreases. It is due to interaction with the boundary layer on the upper wall of the wind tunnel, the stream line pattern changes and the area under the separation zone at the rear side as well as the upper face of the bluff body (*i. e*. square prism) decreases.

Also, from the plot C_D *vs.* angle attack, it is observed that the value of C_D is maximum at an angle of attack $\alpha = 50°$, because in that orientation the area of the bluff body (*i. e.* square prism) is under maximum separation zone.

The uncertainties in Re and C_p have been calculated following the method given by Kline and McClintock [21] and found to be within the range of 3.13% and 4.25%, respectively, in this investigation.

Heat transfer

Information regarding the heat transfer rate from the bluff bodies are of interest to the designers in engineering practice. In the present investigation, experiments have been conducted for various sizes of the square prisms for generating this information under constant heat flux condition. Heat flux has been calculated from the heat input divided by the surface area of the heating foil. Input heat flux has been corrected by subtracting the heat loss per unit area. Heat loss calculation has been done by using the empirical correlation given by Hossain and Brahma [20]. The side length of the prism has been taken as the characteristics length for the definition of the Nusselt number. Local and average Nusselt number have been plotted for various angles of attack, blockage ratios, height-ratios and Reynolds numbers for different models of square prism. Figures 15 and 16 shows the variation of local Nusselt number (Nu_x) with the non-dimensional dis-

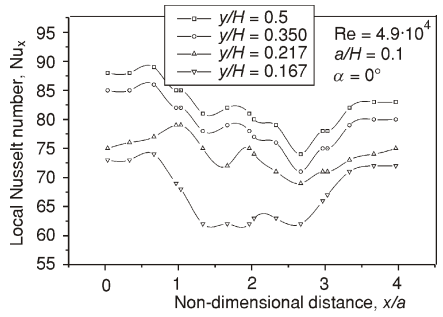

Figure 15. Variation of local Nusselt number with non-dimensional distance at different height-ratios of a square prism (*a/H* = 0.1, $\alpha = 0°$)

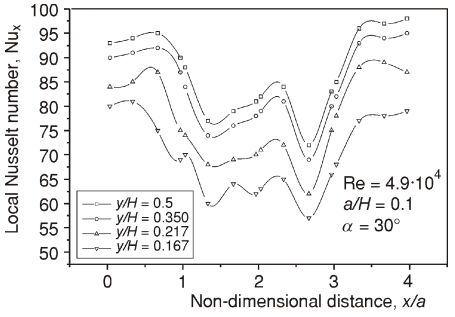

Figure 16. Variation of local Nusselt number with non-dimensional distance at different height-ratios of a square prism (*a/H* = 0.1, $\alpha = 30°$)

tance (x/a) at $\alpha = 0$, and 30°, respectively, where Re = $4.9 \cdot 10^4$ and $a/H = 0.1$. Figure 15 shows values of the local Nusselt number at all points on the surface decreases as the square prism approaches towards the upper wall, *i. e. y/H* decreases. The nature of all graphs (*i. e*. for all *y/H*) first increases very slightly and then afterwards sometimes it increases and then decreases. In, fig. 16, at $\alpha = 30°$, the graph between Nu_x with x/a and the variation in Nusselt numbers is pre-dominant. Figures 17 and 18 shows the variation Nu_x *vs. x/a* for $y/H = 0.5$, 0.350, and 0.217 where Re = $4.9 \cdot 10^4$ and $a/H = 0.2$. In fig. 17, the value of Nu_x first decreases at $x/a = 0.5$ and then there is a very sharp increase and again it decreases and increases continuously. In fig. 18, the curve is at first sharply decreases and then increases but at some points (*i. e*. $x/a = 1.667$, 1.983, 2.017, 2.333, and 2.5) the graph for all *y/H* are almost straight-line type nature and then increases sharply. The value of Nu_x at all x/a decreases while *y/H* decreases *i. e*. the square prism approaches towards the upper wall of the wind tunnel.

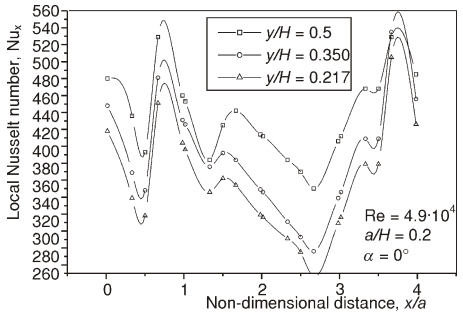

Figure 17. Variation of local Nusselt number with non-dimensional distance at different height-ratios of a square prism ($a/H = 0.2$, $\alpha = 0°$)

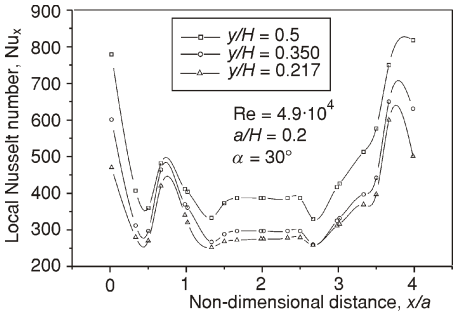

Figure 18. Variation of local Nusselt number with non-dimensional distance at different height-ratios of a square prism ($a/H = 0.2$, $\alpha = 30°$)

Figures 19 and 20 shows the plot of local Nusselt number with non-dimensional distance for $y/H = 0.5$, 0.350, and 0.217 where Re = $4.9 \cdot 10^4$, $a/H = 0.3$. For all figures, the variation of Nu_x at some points x/a is quite sharply increases or decreases. In fig. 19, the value of Nu_x decreases while height-ratio *y/H* decreases but the variations are very less between the height-ratios. At $x/a = 1.611$, the value of Nu_x is maximum for all *y/H*. In fig. 20, (*i. e*. $\alpha = 30°$), the variation of Nu_x for all *y/H* is very less, moreover for $y/H = 0.5$ and 0.350, the values of Nu_x at all points of thermocouples are almost same. The val-

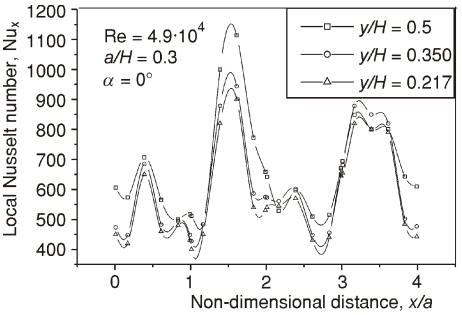

Figure 19. Variation of local Nusselt number with non-dimensional distance at different height-ratios of a square prism ($a/H = 0.3$, $\alpha = 0°$)

ues of Nu_x at x/a = 2.389 and 3.611 are maximum. Figures 21 and 22 shows Nu_x *vs*. x/a at y/H = 0.5 and = 0.350 for Re = $4.9 \cdot 10^4$, a/H = 0.4. In fig. 21, the value of Nu_x is minimum at x/a = 0.875 for y/H = 0.5 and x/a = 0.625 for y/H = 0.350 and then increases and decreases markedly. In fig. 22, the values of local Nusselt number are minimum at x/a = 1.0083 and maximum at x/a = 3.875 for both y/H. For both figures, the values of Nu_x for all x/a are higher for y/H = 0.5 than that of y/H = 0.350.

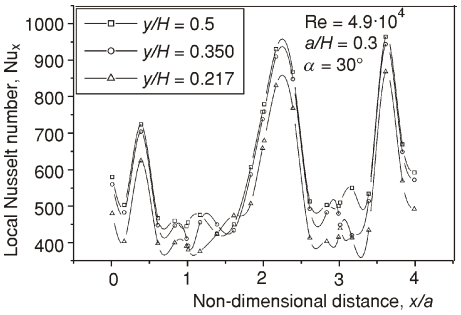

Figure 20. Variation of local Nusselt number with non-dimensional distance at different height-ratios of a square prism (a/H = 0.3, α = 30°)

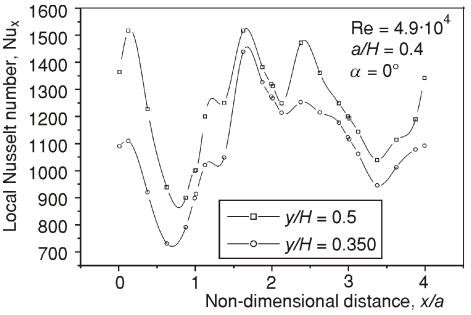

Figure 21. Variation of local Nusselt number with non-dimensional distance at different height-ratios of a square prism (a/H = 0.4, α = 0°)

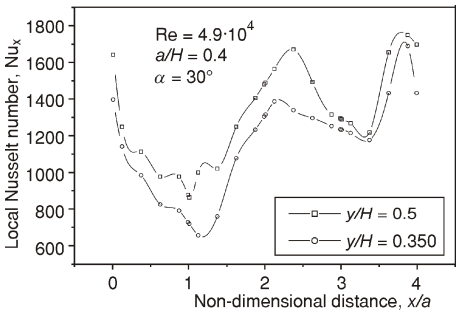

Figure 22. Variation of local Nusselt number with non-dimensional distance at different height-ratios of a square prism (a/H = 0.4, α = 30°)

Average Nusselt numbers has been calculated by this procedure. Firstly, the value of Nu_x has been integrated for all four faces separately and then added and divided by four to get the average value of Nu_a. Figures 23 and 24 shows the plot of Nu_a with various angles of attacks α for different height-ratios where the blockage ratios a/H are equal to 0.1 and 0.2, respectively, and Re = $4.9 \cdot 10^4$. The maximum value of Nu_a has been observed at α = 70° for both figures. Figures 25 and 26 shows the plot of Nu_a with different angles of attacks α for various height-ratios where the blockage ratios a/H are equal to 0.3 and 0.4 respectively, and Re = $4.9 \cdot 10^4$. In fig. 25, the Nu_a increases from α = 0-20° and then decreases up to α = 60° and again the value of Nusselt number increases. The maximum value of Nu_a has been observed at α = 50° in fig. 26, except at y/H = 0.350, the maximum value occurs at α = 70°. For all the plots of Nusselt number with angle of attack, the average value of Nu_a for all α decreases as the square prism approaches towards the upper wall *i. e*. y/H decreases.

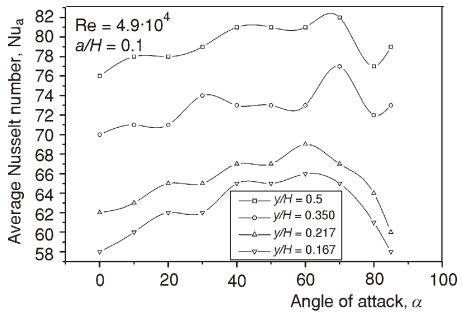

Figure 23. Variation of average Nusselt number with angle of attack at different height-ratios of a square prism (*a/H* = 0.1)

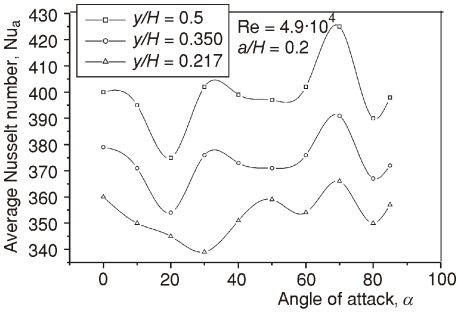

Figure 24. Variation of average Nusselt number with angle of attack at different height-ratios of a square prism (*a/H* = 0.2)

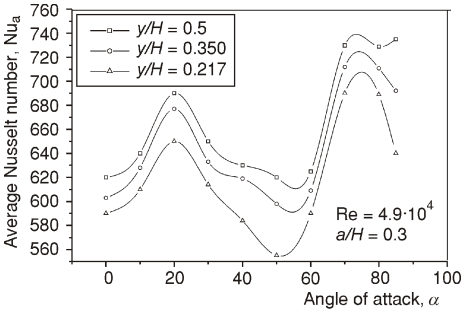

Figure 25. Variation of average Nusselt number with angle of attack at different height-ratios of a square prism (*a/H* = 0.3)

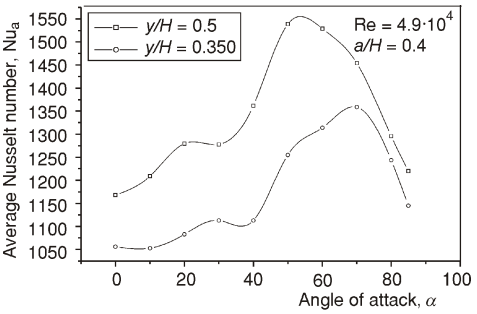

Figure 26. Variation of average Nusselt number with angle of attack at different height-ratios of a square prism (*a/H* = 0.4)

Regarding the heat transfer experiment, the value of local heat transfer coefficient decrease as the body approaches towards the upper wall of the wind tunnel as the area under separation zone decreases. But it is really difficult to explain about the characteristics of heat transfer phenomena under flow separation zone. Basically it depends upon the behavior of the local fluid mechanics *i. e*. velocity and static pressure distributions at a particular location at that moment.

The uncertainties in local heat transfer coefficient and local Nusselt number have been calculated [21] and found to be within the range of 4.52 % and 5.25%, respectively.

Conclusions

The following conclusions can be made for square prisms from the results of the experiments.

The pressure coefficient (C_p) shows positive values on the front face whereas the rear face is within separated flow region for all angles of attack.

The values of positive pressure coefficients for all blockage ratios are almost it at all points on the surface of the prisms at different height-ratios.

The values of negative pressure coefficients for all blockage ratios and Reynolds numbers increases for almost all points on the surface as the bluff body approaches towards the upper wall of the wind tunnel.

The values of drag coefficient (C_D) for all angles of attack, Reynolds numbers and blockage ratios decreases as the prism moves in the direction of the upper wall of the wind tunnel.

The maximum value of drag coefficient is observed at an angle of attack nearly 50° for all blockage ratios and Reynolds numbers in case of the square prism.

The local Nusselt number for all blockage ratios decreases as the value of height-ratio decreases for almost all points on the surface as the prism approaches towards the upper wall of the wind tunnel.

The values of average Nusselt number (Nu_a) for all angles of attack, Reynolds numbers, and blockage ratios decreases as the prism moves in the direction of the upper wall of the wind tunnel.

There is no definite angle of attack for all blockage ratios and Reynolds numbers at which the value of average Nusselt number is either maximum or minimum.

Nomenclature

A – surface area of the bluff body, [m^2]
a – side length of the square prism, [mm]
a/H – blockage ratio of the square prism, [–]
C_D – drag coefficient [$= F_D/(0.5\rho_a u^2 A)$], [–]
C_p – pressure coefficient [$= (p - p_a)/(0.5\rho_a u^2)$], [–]
F_D – drag force, [N]
H – height of the wind tunnel, [mm]
h_a – average heat transfer coefficient, [$Wm^{-2}K^{-1}$]
h_x – local heat transfer coefficient, [$Wm^{-2}K^{-1}$]
k – thermal conductivity, [$Wm^{-2}K^{-1}$]
Nu_a – average Nusselt number ($= h_a a/k$), [–]
Nu_x – local Nusselt number ($= h_x a/k$), [–]
p – static pressure, [mm of water]
p_a – ambient pressure, [mm of water]
Re – Reynolds number based on the velocity of air and the characteristics length of the bluff body ($= ua/\nu_a$), [–]
u – velocity of air, [ms^{-1}]
x – distance along the perimeter starting from the corner A of the prism, [mm]
x/a – distance for the square prism, [–]
y – distance of the centroid of the bluff body from the upper wall of the wind tunnel, [mm]
y/H – height-ratio, [–]

Greec letters

α – angle of attack, [°]
β – Coefficient of thermal expansion, [K^{-1}]
ρ_a – density of air, [kgm^{-3}]
ν_a – kinematic viscosity of air, [m^2s^{-1}]

References

[1] Bearman, P. W., Investigation of Flow behind a Two Dimensional Model with Blunt Trailing Edge and Fitted with Splitter Plates, *Journal of Fluid Mechanics, 21* (1965), Part 2, pp. 241-255
[2] Bearman, P. W., Trueman, D. M., An Investigation of the Flow Around Rectangular Cylinders, *Aeronautical Quarterly, 23* (1972), August, pp. 229-237
[3] Aplet, C. J., *et. al.,* The Effects of Wake Splitter Plates on the Flow Past a Circular Cylinder in the Range $10^4 < Re < 5 \cdot 10^4$, *Journal of Fluid Mechanics, 61* (1973), Part 1, pp. 187-198
[4] Bearman, P. W., Zdravkovich, M. M., Flow Around a Circular Cylinder Near a Plane Boundary, *Journal of Fluid Mechanics, 89* (1978), Part 1, pp. 53-73
[5] Igarashi, T., Characteristics of the Flow Around a Square Prism, *Bull JSME, 27* (1984), 231, pp. 1858-1864
[6] Igarashi, T., Characteristics of Flow Around Rectangular Cylinders, *Bull. JSME, 28* (1985), 242, pp. 1690-1696
[7] Mansingh, V., Oosthuizen, P. H., Effects of Splitter Plates in the Wake Flow Behind a Bluff Body, *AIAA Journal*, *28* (1990), 5, pp. 778-783
[8] Simpson, R. L., The Structure of the Near Wall Region of Two Dimensional Turbulent Separated Flow, *Phils Trans. R. Soc. Lond., Serie A, 336* (1991), pp. 5-17
[9] Igarashi, T., Heat Transfer in Separated Flows, *Proceedings*, 5th International Heat Transfer Conference, Tokyo, 1974, pp. 300-304
[10] Igarashi, T., *et. al*., Heat Transfer in Separated Flows, Part 1. Experiments on Local Heat Transfer from the Rear of a Flat Plate to an Air Steam, *Heat Transfer Japanese Research, 4* (1975), 1, pp. 11-32
[11] Igarashi, T., Hirata, M., Heat Transfer in Separated Flows, Part 3. The Case of Equilateral Triangular Prisms, *Heat Transfer Japanese Research, 6* (1977), 4, pp. 13-39
[12] Igarashi, T., Heat Transfer in Separated Flows, Part 2. Theoretical Analysis, *Heat Transfer Japanese Research, 6* (1977), 3, pp. 60-78
[13] Igarashi, T., Fluid Flow and Heat Transfer in the Separated Region of a Circular Cylinder with Wake Control, *Heat Transfer Japanese Research, 11* (1982), 3, pp. 1-16
[14] Igarashi, T., Correlation between Heat Transfer and Fluctuating Pressure in Separated Region of a Circular Cylinder, *Int. J. Heat Mass Transfer, 27* (1984), 6, pp. 927-937
[15] Igarashi, T., Heat Transfer from a Square Prism to an Air Stream, *Int. J. Heat Mass Transfer, 28* (1985), 1, pp. 175-181
[16] Aiba, S., Tsuchoda, H., Heat Transfer Around a Circular Cylinder Near a Plane Boundary, *Trans JSME, 51-463,* 1985, pp. 866-873
[17] Igarashi, T., Local Heat Transfer from a Square Prism to an Air Stream, *Int. J. Heat Mass Transfer, 29* (1986), 5, pp. 777-784
[18] Igarashi, T., Fluid Flow and Heat Transfer Around Rectangular Cylinders, *Int. J. Heat Mass Transfer, 30* (1987), 5, pp 893-901
[19] Yovanovich, M. M., Refai, A. G., Experimental Study of Forced Convection from Isothermal Circular and Square Cylinders and Toroids, *Journal of Heat Transfer, Trans. ASME, 119* (1997), February, pp. 70-79

[20] Hossain, A., Brahma, R. K., Experimental Investigations of Fluid Flow and Heat Transfer Characteristics of a Slot Jet Impinging on a Square Cylinder, *Wärme and Stoffübertragung, 28* (1993), 7, pp. 381-386
[21] Kline, S. J., McClintock, F. A., Describing Uncertainties in Single-Sample Experiments, *Mechanical Engineering, 75* (1953), 1, pp. 3-8

Authors' addresses:

D. Chakrabarty
MCKV Institute of Engineering, Department of Automobile Engineering
Liluah-711204, West Bengal, India

R. Brahma
Indian Institute of Technology, Department of Mechanical Engineering
Kharagpur-721302, West Bengal, India

Corresponding author D. Chakrabarty
E-mail: dipes_chak@yahoo.co.in

Paper submitted: November 11, 2006
Paper revised: May 22, 2007
Paper accepted: October 8, 2007